THE JOURNAL OF BIOLOGICAL CHEMISTRY
Vol. 278, No. 19, Issue of May 9, pp. 17455–17465, 2003
Printed in U.S.A.

Cytochrome *c* Nitrite Reductase from *Desulfovibrio desulfuricans* ATCC 27774

THE RELEVANCE OF THE TWO CALCIUM SITES IN THE STRUCTURE OF THE CATALYTIC SUBUNIT (NrfA)*

Received for publication, November 19, 2002, and in revised form, January 16, 2003
Published, JBC Papers in Press, March 4, 2003, DOI 10.1074/jbc.M211777200

Carlos A. Cunha‡, Sofia Macieira§, João M. Dias‡, Gabriela Almeida‡¶, Luisa L. Gonçalves‡¶, Cristina Costa‡, Jorge Lampreia‡, Robert Huber§, José J. G. Moura‡, Isabel Moura‡, and Maria João Romão‡‖

From the ‡Rede de Química e Tecnologia (REQUIMTE) Centre de Química Fina e Biotecnologia (CQFB), Departamento de Química, Faculdade de Ciências e Tecnologia, Universidade Nova de Lisboa, 2829-516 Caparica, Portugal, the ¶Instituto Superior de Ciências da Saúde-Sul, Campus Universitário Quinta da Granja, 2825-511 Caparica, Portugal, and the §Max-Planck-Institut für Biochemie, Abteilung Strukturforschung, Am Klopferspitz 18a, 82152 Martinsried, Germany

The gene encoding cytochrome *c* nitrite reductase (NrfA) from *Desulfovibrio desulfuricans* ATCC 27774 was sequenced and the crystal structure of the enzyme was determined to 2.3-Å resolution. In comparison with homologous structures, it presents structural differences mainly located at the regions surrounding the putative substrate inlet and product outlet, and includes a well defined second calcium site with octahedral geometry, coordinated to propionates of hemes 3 and 4, and caged by a loop non-existent in the previous structures. The highly negative electrostatic potential in the environment around hemes 3 and 4 suggests that the main role of this calcium ion may not be electrostatic but structural, namely in the stabilization of the conformation of the additional loop that cages it and influences the solvent accessibility of heme 4. The NrfA active site is similar to that of peroxidases with a nearby calcium site at the heme distal side nearly in the same location as occurs in the class II and class III peroxidases. This fact suggests that the calcium ion at the distal side of the active site in the NrfA enzymes may have a similar physiological role to that reported for the peroxidases.

In *Desulfovibrio desulfuricans*, as happens in other proteobacteria, cytochrome *c* nitrite reductase was shown to be the terminal enzyme in the anaerobic respiratory pathway using nitrate or nitrite as terminal electron acceptors (Refs. 1–3, see Refs. 4–6 for reviews). This is a process making part of the biogeochemical nitrogen cycle that may start with the reduction of nitrate to nitrite catalyzed by nitrate reductase (NapA) (7), followed by the six-electron reduction of nitrite to ammonia catalyzed by the five-heme cytochrome *c* nitrite reductase. This electron transport chain is located at the periplasmic membrane. Mutation studies in the operon encoding cytochrome *c* nitrite reductase from *Wolinella succinogenes* suggest that these enzymes are not integral membrane proteins but they are anchored to the membrane by a second subunit (NrfH) encoded in the same operon (8), a NapC/NirT-type cytochrome *c* that has been suggested also to mediate the electron transfer between the membranous menaquinone pool and the catalytic unit (9).

Crystal structures have been determined for the catalytic subunit of cytochrome *c* nitrite reductase (NrfA) from the ϵ-proteobacteria *Sulfurospirillum deleyianum* (10) and *Wolinella succinogenes* (11) and, more recently, from the γ-proteobacterium *Escherichia coli* (12). These enzymes are homologous and share a highly conserved three-dimensional structure. The sequence of *W. succinogenes* NrfA is 75% identical to the one from *S. deleyianum,* whereas *E. coli* NrfA is 48 and 46% identical with the ones from *W. succinogenes* and *S. deleyianum*, respectively. The crystal structures of these enzymes show the same homodimeric structure, the same packing for the five *c*-type heme groups within each monomer, and the same environment at the active site, localized at heme 1, an unusual lysine-coordinated heme with the distal coordination position free to accommodate the substrate molecule. Biochemical studies suggest that the homodimer is the functional form of the catalytic unit (13). In all these structures, a conserved calcium ion (calcium I) with octahedral coordination is present near the active site.

Here we report the crystal structure of the catalytic subunit of cytochrome *c* nitrite reductase from *D. desulfuricans* ATCC 27774, a 61-kDa protein encoded by the *nrf*A gene (14–16). This is the first structure of this family of enzymes from a δ-proteobacterium, and it reveals considerable structural differences relative to the previously reported structures. A second calcium site (calcium II) with nearly perfect octahedral coordination, caged by a loop not existent in the previous structures, was identified coordinating the propionates A of hemes 3 and 4. This calcium ion is located at nearly the same position as a yttrium and calcium ions bound at the protein surface in the crystal structures of NrfA from *W. succinogenes* and *E. coli*, respectively. However, in these cases, the ions presented incomplete coordination shells and no physiological relevance

* This work was supported by Fundo Social Europeu (FSE) and FCT (Fundação para a Ciência e Tecnologia) through Ph.D. grants PRAXIS XXI/BD/15752/98 (to C. A. C.), PRAXIS XXI/BD/13530/97 (to J. M. D.), PRAXIS XXI/BD/16009/98 (to S. M.), and PRAXIS XXI/BD/11349/97 (to G. A.), the European Co-operation in the Field of Science and Technology (COST) working group, and support for measurements at the European Synchrotron Radiation Facility under the European Union TMR/LSF Program. The costs of publication of this article were defrayed in part by the payment of page charges. This article must therefore be hereby marked "*advertisement*" in accordance with 18 U.S.C. Section 1734 solely to indicate this fact.

The atomic coordinates and structure factors (code 1oah) have been deposited in the Protein Data Bank, Research Collaboratory for Structural Bioinformatics, Rutgers University, New Brunswick, NJ (http://www.rcsb.org/).

‖ To whom correspondence should be addressed. Tel.: 351-21-2948310; Fax: 351-21-2948385; E-mail: mromao@dq.fct.unl.pt.

TABLE I
MAD data processing and phasing statistics

Wavelength	Resolution limit	Completeness	R_{merge}	$I/\sigma(I)$	f'	f''	Phasing power$_{Iso}$	Phasing power$_{ano}$	R_{Cullis}
Å		%							
1.7403	2.7	95.1 (91.5)[a]	0.09 (0.20)	6.9 (3.4)	−10.8	3.0	2.14	1.08	72.1
1.7390	2.7	94.9 (84.5)	0.09 (0.21)	7.3 (3.2)	−11.1	2.0	2.24	0.92	68.3
0.9919	2.5	96.2 (85.2)	0.04 (0.12)	14.6 (5.6)	0.24[b]	1.53[b]		1.20	

[a] Values in parentheses refer to the last resolution shell.
[b] Indicates that the values were not refined.

had been assigned to them. In the present work, the physiological role of the two calcium sites present in *D. desulfuricans* NrfA is discussed.

EXPERIMENTAL PROCEDURES

Gene Sequence Determination—The NrfA internal peptides AETETKM and KAEQWEGQDR obtained by automated Edman degradation[1] were used to design the degenerate primers: Nir-AETETKM, 5′-GCIGARACIGARACIAARATG-3′, and Nir-Cterm, 5′-TCYTGIC-CYTCCCASACYTGYTC-3′. Using these oligonucleotides a DNA fragment of about 1431 base pairs was amplified by PCR. The resulting product was cloned in the vector pPCR-Script™ Amp SK(+) (Stratagene) and sequenced in both strands with primers T3 and T7 (New England Biolabs) and with internal primers, using an automated DNA sequencer (model 373, Applied Biosystems, Foster City, CA) and the PRISM ready reaction dye deoxyterminator cycle sequencing kit (Applied Biosystems). More information on the N terminus was gained after identification and sequencing of the gene encoding the small subunit.[1] The presence of a signal peptide was checked with the program Signal P V1.1[2] (18).

Protein Purification and Crystallization—D. desulfuricans NrfA was extracted by mild treatment of the membrane fraction with sodium choleate (4–6 mg/liter) in 0.1 M potassium phosphate buffer at pH 7.6, as previously described (15). The enzyme was purified by sequential ammonium sulfate fractionation (30–60%), resuspension in potassium phosphate buffer, and high performance liquid chromatography/gel filtration on a Superdex 200 (Amersham Biosciences) column equilibrated and eluted with 0.1 M potassium phosphate buffer at pH 7.6. The purity was checked by UV-visible spectroscopy and by SDS-polyacrylamide mini-gel (12.5%) electrophoresis according to the Laemmli method (19). Despite the fact that NrfA enzymes are not integral membrane proteins but anchored to the membrane by the second subunit, crystals of *D. desulfuricans* NrfA could only be obtained using detergents in the crystallization conditions (20). Single crystals of dimensions 0.3 × 0.15 × 0.15 mm suitable for x-ray diffraction studies were grown for 1 month using 3-(decylmethylammonium)propane-1-sulfonate (Zwittergent 3-10 from Calbiochem) added to the crystallization conditions as a solution with a concentration of about 10 times the critical micellar concentration (40 mM). The crystallization conditions contained 15% (w/v) PEG 3350, 0.2 M $CaCl_2$, and 0.1 M HEPES buffer at pH 7.5. The protein was used at a concentration of 10 mg/ml. The crystals were obtained by the vapor diffusion method with hanging drop. The drops were prepared by adding 4 μl of protein solution, 1 μl of detergent at 10 times the critical micellar concentration, and 5 μl of reservoir solution.

Multiple Wavelength Anomalous Dispersion (MAD)[3] Phasing—A cryo-cooled single crystal of dimensions 0.3 × 0.15 × 0.15 mm^3 was used to collect MAD data at the iron absorption edge, on beamline BM-14 at the European Synchrotron Radiation Facility, Grenoble, France. Ethylene glycol added at a concentration of 25% to the crystallization solution was used as cryoprotectant and the crystal was cryo-cooled to 100 K in a flux of nitrogen gas. The wavelengths at the point of inflection and at the peak of the K-shell absorption edge of iron were determined to be λ_1 = 1.7403 Å and λ_2 = 1.7390 Å, respectively, from an x-ray fluorescence spectrum. Data sets were collected at these wavelengths with a resolution up to 2.7 Å, using a MAR 345 image plate detector. The remote wavelength data set was collected at λ_3 = 0.9919 Å, up to a resolution of 2.5 Å. Data were processed using version 1.96.1 of programs DENZO and SCALEPACK (21). The crystals belong to the space group $P2_12_12_1$ with unit cell constants a = 78.94 Å, b = 104.59 Å, and c = 143.18 Å. The statistics of data processing are presented in Table I. Using the program SOLVE (22), 10 iron sites were found in the asymmetric unit and phases were obtained with the program SHARP (23), resulting in a phasing power of 2.24 and an overall figure of merit of 0.49 (Table I). Density modification was performed with programs SOLOMON (24) (solvent flattening) and DM (25, 26) (solvent flattening and averaging). At this stage, the protein boundaries, the helical regions at the dimer interface, and the heme cofactors could be distinguished in the electron density maps. However, large regions of the protein showed highly discontinuous electron density that did not improve much with the density modification procedures, making difficult the task of model building in those regions. Because at this stage the primary sequence was not yet known and the related *S. deleyianum* NrfA structure was available, attempts to solve the structure by molecular replacement were done in parallel.

TABLE II
Refinement statistics

Wavelength (Å)	0.932
Resolution range (Å)	20.0–2.3
Number of independent reflections	51633
$I/\sigma(I)$ (last shell)	11.7 (2.2)
Completeness (last shell)	97.3 (89.8)
R_{merge} (last shell)	0.08 (0.39)
Number of amino acid residues (waters)	964 (498)
Number of hemes	10
Number of calcium ions	4
Number of chloride ions	3
Number of zinc ions	1
Average B-factor for protein atoms (water) (Å^2)	27.6 (29.1)
Root mean square deviation in bond lengths (Å)	0.008
Root mean square deviation in bond angles (degrees)	1.378
Crystallographic R_{factor} (R_{free})	0.189 (0.224)

Structure Solution by Molecular Replacement—A solution of the structure was obtained by molecular replacement using the program AMoRe (27, 26). The data set used in this case, with a resolution up to 2.3 Å, was collected from a crystal similar to the one used in the MAD experiment, using radiation at λ_4 = 0.932 Å, on beamline ID14-EH4 at the European Synchrotron Radiation Facility and using the local 2 × 2 array of ADSC CCD detectors. The structure of *S. deleyianum* NrfA (10) was used as a search model. The solution was obtained using the model comprising the residue ranges 60 to 140, 150 to 217, 239 to 304, 319 to 490, and hemes 1, 3, and 4. Heme 2, located in an exposed and flexible region of the protein, and heme 5, located at the dimer interface, were not included in the search model because there could be significant shifts in their position and orientation between the model and the *D. desulfuricans* NrfA structure as was found to be true for heme 2 after solving the structure (see Fig. 3*A*). A dimer was found in the asymmetric unit that corresponds to a Matthews volume (28) of 2.3 Å^3 Da^{-1} and in agreement with the 10 iron sites found in the asymmetric unit by the MAD experiment. The MR solution has a R-factor of 51.9% and a correlation of 36.9%, in the resolution range between 10.0 and 3.0 Å, which is a high R-factor accompanied by a low correlation. However, the MR solution could superimpose well on the electron density maps obtained by MAD if its coordinates were shifted half a unit cell along the a axis that corresponds to an alternative allowed origin in space group $P2_12_12_1$.

Model Building and Refinement—Model building was done with program O (29) and refinement was carried out with program REFMAC (26, 30). The initial model obtained by MR was corrected accordingly to the electron density maps calculated after rigid body refinement and also by comparison to the ones calculated using the experimental phases determined by MAD. Hemes 2 and 5 as well as the calcium ion

[1] M. G. Almeida, S. Macieira, L. L. Gonçalves, R. Huber, C. A. Cunha, M. J. Romão, C. Costa, J. Lampreia, J. J. G. Moura, and I. Moura, submitted for publication.
[2] www.cbs.dtu.dk.
[3] The abbreviations used are: MAD, multiple wavelength anomalous dispersion; H-bond, hydrogen-bond; MR, molecular replacement; ncs, non-crystallographic symmetry.

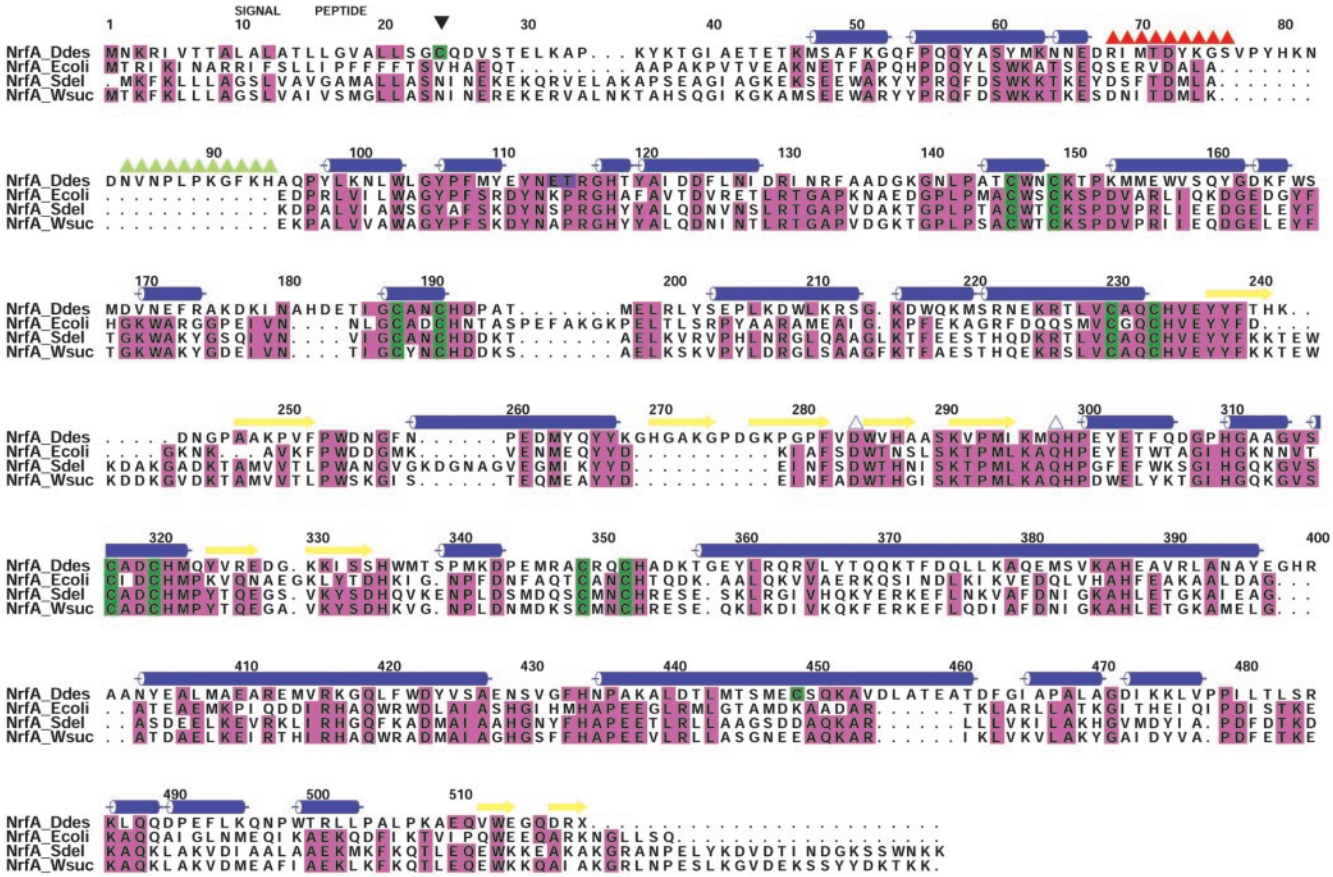

FIG. 1. **Amino acid sequence alignment.** NrfA_Ddes, NrfA from *D. desulfuricans* ATCC 27774 (EMBL accession number AJ316232); NrfA_Ecoli, NrfA from *E. coli* (SWISS-PROT accession number P32050); NrfA_Sdel, NrfA from *S. deleyianum* (SWISS-PROT accession number Q9Z4P4); NrfA_Wsuc, NrfA from *W. succinogenes* (TREMBL accession number Q9S1E5). Conserved residues are colored in *pink*, cysteines are in *green*, and calcium II ligands are in *violet*. The meanings of the symbols are: *black inverted triangle*, probable signal peptide cleavage site; *white triangles*, calcium I ligands; *red triangles*, residues forming the loop L1 that cages calcium II; *green triangles*, residues forming the loop L2 that hinders the product outlet; *blue cylinders*, α-helices; *yellow arrows*, β-strands. Numbering and positioning of the secondary structural elements refer to the NrfA_Ddes sequence. This figure was prepared with the programs PILEUP, in the Wisconsin Package version 10.0 (Genetics Computer Group (GCG), Madison, WI) and ALSCRIPT (51).

near the active site were incorporated in the model obtained by MR, and the residue ranges of the model were corrected to the following regions: 56 to 151, 153 to 222, 234 to 244, 252 to 263, 266 to 308, 315 to 377, and 385 to 441. At this point it could already be observed that the last 73 residues in the C terminus region of the *S. deleyianum* NrfA structure did not follow the electron density and, for this reason, they were removed from the initial model. The side chains that did not fit the electron density were mutated to alanines. Refinement of the model thus obtained, with inclusion of the experimental phases from MAD, lowered the *R*-factor to 44.1% in the resolution range between 14.5 and 2.5 Å. During the early stages of model building, until the *R*-factor decreased to below 40%, refinements were carried out including the experimental phases from MAD. Following the refinement with program REFMAC, the program ArpWarp (31) was used in mode molrep, not including the experimental phases and using data in the resolution range between 14.5 and 2.3 Å. Model building was performed using the improved electron density maps obtained from ArpWarp until the *R*-factor of the protein model decreased to below 30% when refined with program REFMAC after model building. During the last stages of model building, refinement was carried out with the program REFMAC5. The *R*-free calculation was done using 1% of the reflections. The stereochemical quality of the final refined model was analyzed with WHATCHECK (32). The final model of the dimer was refined to a *R*-factor of 18.9% and *R*-free of 22.4% and refinement statistics are summarized in Table II. Each monomer is composed of 482 residues (sequence residues 38 to 519), five *c*-type heme groups, two calcium ions, and one chloride ion. One of the monomers in the asymmetric unit binds one zinc ion with one additional chloride ion as one of its ligands, which corresponds to a tetrahedral metal center that was identified at an intermolecular contact between crystallographic symmetry related copies of that monomer. Electron density corresponding to at least one more amino acid after residue 518, in the C terminus, could be seen in the maps. However, more amino acids after residue 518 could not be detected during the sequence determination. For this reason, residue 519 is present as an alanine in the crystal structure. There was no electron density corresponding to the residues from 325 to 331 in monomer A, suggesting that this region was disordered in the crystal. The final model has 498 water molecules, 174 of which have a non-crystallographic symmetry-related mate. The model coordinates have been deposited in the Protein Data Bank with the accession code 1oah.

RESULTS

Primary Sequence—A sequence alignment performed with the amino acid sequences of the known cytochrome *c* nitrite reductases and with the NrfA internal peptides AETETKM and KAEQWEGQDR allowed the identification of these two sequences as portions of NrfA N and C terminus, respectively. The designed oligonucleotides were used to amplify by PCR a DNA fragment of about 1431 base pairs containing part of the *nrf*A gene sequence. The identification of the gene encoding the small subunit (*nrf*H) located upstream of *nrf*A allowed the identification of the NrfA N-terminal sequence. The encoded NrfA is a 518-residue polypeptide chain harboring a signal peptide targeting protein export to the periplasm. According to the program Signal P (18) this peptide is predicted to be 28 residues long, but N-terminal sequencing of the protein[1] indicates that the cleavage site should be located between positions 24 and 25 (Fig. 1). Further attempts to identify the sequence located downstream of *nrf*A were not successful, so the stop

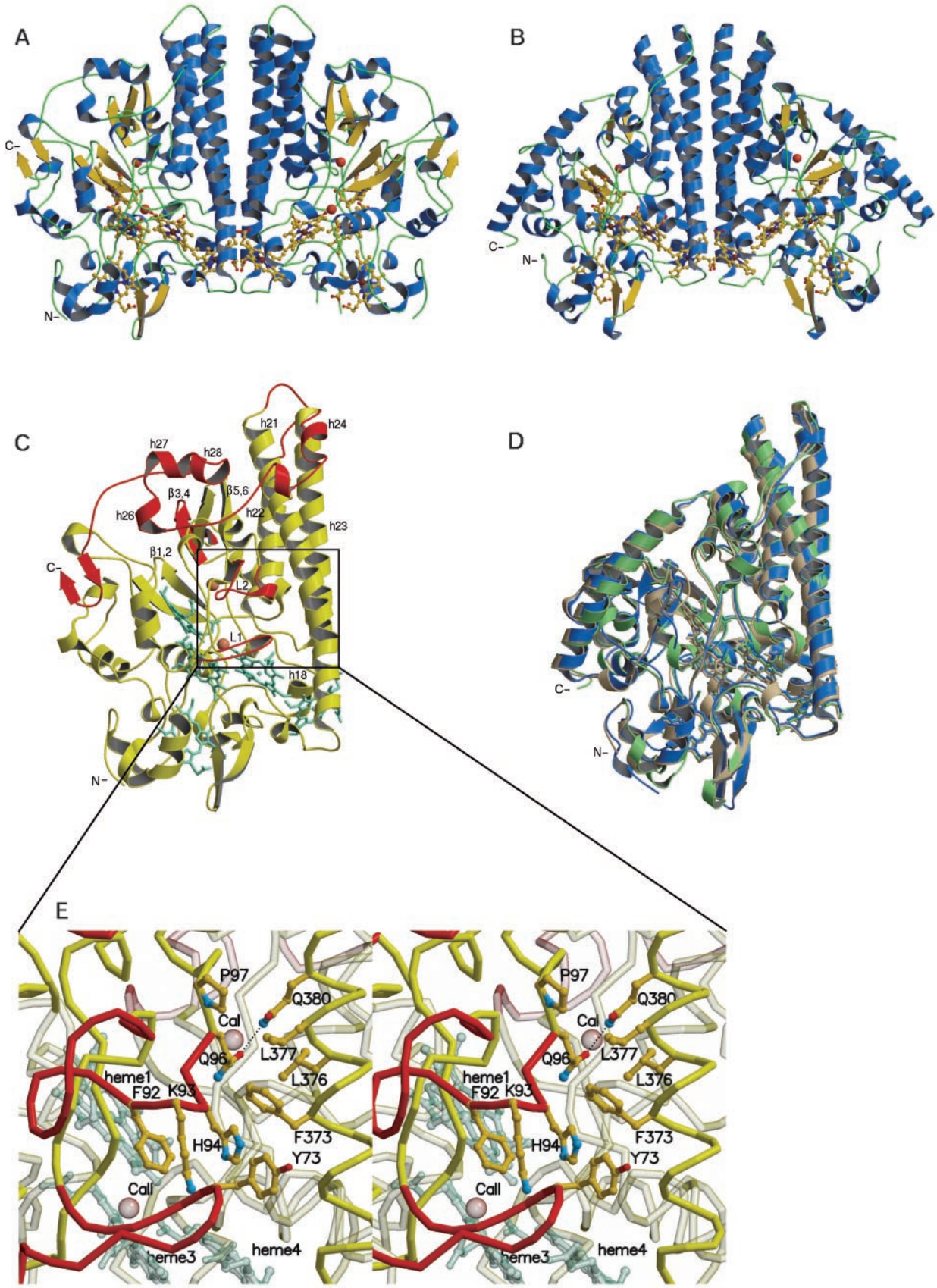

FIG. 2. **Structure of *D. desulfuricans* NrfA and comparison with the previous NrfA structures.** *A*, view of the dimer structure of *D. desulfuricans* NrfA showing the two monomers related by a non-crystallographic dyad. *B*, view of the dimer structure of *E. coli* NrfA, the NrfA structure with highest structural homology to *D. desulfuricans* NrfA. The orientation is the same as in *A*, for comparison. *C*, one monomer of *D. desulfuricans* NrfA showing conserved (*yellow*) and non-conserved (*red*) regions relatively to the previous NrfA structures in the same orientation as in *A*. The non-conserved regions in *D. desulfuricans* NrfA are located around the substrate inlet, the product outlet, and the top edge of the interacting region at the dimer interface. Residues 68 to 76 and 84 to 94 form the additional loops L1 and L2, respectively. *D*, superposition

codon was not identified and the gene was considered to be only partially sequenced. The *nrf*A sequence has been submitted to the EMBL data base under accession number AJ316232. The mature NrfA polypeptide chain is then composed of 494 residues according to the *nrf*A sequence, but it can be one residue longer, as shown by the electron density maps from x-ray crystallography. The polypeptide chain in the crystal structure begins at residue Thr-38 suggesting that the initial amino acids in the N-terminal region of the mature enzyme are disordered. *D. desulfuricans* NrfA is homologous to its counterparts with known structure (Fig. 1) but its shared identity at the primary structure level is relatively low, with a degree of sequence identity of 35.9, 34.3, and 32.9% relatively to the cytochrome *c* nitrite reductases from *S. deleyianum*, *E. coli*, and *W. succinogenes*, respectively.

Overall Structure—The structure of *D. desulfuricans* NrfA (Fig. 2*A*) follows the typical dimer structure of the NrfA family of enzymes (Fig. 2*B*), which is believed to be the active form of the enzyme (13). The monomers are related in the dimer by a 2-fold ncs axis and they are structurally homologous to the previous NrfA structures but to a lesser degree in this case (Fig. 2, *C* and *D*). The conserved regions correspond to 77% of the total number of amino acid residues with a root mean square deviation of 1.7 Å in relation to the NrfA from *E. coli* (for the main chain atoms of 370 residues) and a root mean square deviation of 2.0 Å in relation to the NrfA from *W. succinogenes* (for the main chain atoms of 372 residues).

The structure is dominated by the conserved characteristic three-helix bundle in the region at the dimer interface (*h21*, *h22*, and *h23* in Fig. 2*C*). Helix h21 shows a kink at residue Thr-368 where its main chain nitrogen atom is H-bonded to the main chain carbonyl group of Val-365 changing the α-helical structure to a 3_{10} helical geometry in this region. On the other hand, helices h22 and h23 are straight along their extension. In the case of h22 this is made possible by the fact that the loop connecting helices h21 and h22 is longer than in the other NrfA structures where it is found that the N terminus of helix h22 bends toward the C terminus of helix h21.

The packing of the five *c*-type heme groups and their axial ligands are similar to what has been observed in the NrfA enzymes (Fig. 3*A*). Hemes 2 to 5, according to the order of their binding motifs in the sequence, are *bis*-histidinyl-coordinated and are most probably used by the enzyme to store and transfer electrons to the active site. Heme 1, which constitutes the active site, is coordinated by a lysine side chain at the proximal side, whereas the iron coordination position at the distal side is vacant. The distances separating the hemes are sufficiently short to allow direct electron transfer between them (33) including electron transfer between the monomers through both hemes 5 at the dimer interface that interact directly with each other by their propionates. The characteristic calcium ion near the active site (calcium I) is also present in *D. desulfuricans* NrfA but, in this case, there is a very clear second calcium ion (calcium II) with octahedral coordination to protein ligands near the propionates of hemes 3 and 4 (as described below).

The most significant structural differences relative to the previous NrfA structures occur in the regions of the sequence contiguous to the N and C termini. These regions are involved at the dimer interface as well as surrounding the putative substrate inlet and product outlet (Fig. 2*C*). Near the N-terminal region, residues 68 to 76 form an additional loop (loop L1 in Fig. 2*C*) that is responsible for the caging and octahedral coordination of the second calcium site (calcium II). Following this loop, residues 84 to 94 form another additional polypeptide segment that blocks partially the product outlet as described below (loop L2 in Fig. 2*C*). The structure at the C-terminal region, comprising residues 463 to 519, is also not conserved. Residues 465 to 470 in this region form a short additional helix (h24 in Fig. 2*C*) involved in the interaction at the dimer interface, followed by a long loop connecting a one turn α-helix, and three short 3_{10} helices (h26, h27, and h28) in a two-elbow arrangement and ending in a short anti-parallel β-sheet at the C terminus. The characteristic long curved α-helix found in the other NrfA structures at the C terminus, which surrounds one side of the substrate inlet, is not present in this case (Fig. 2, *C* and *D*).

The electrostatic potential at the surface of the protein is dominated by the positively charged region around the channel leading to the active site (Fig. 3*C*) and by the negative electrostatic potential around the putative product outlet. These electrostatic features, conserved in this family of enzymes, are considered to be important to attract the negatively charged nitrite ions to the active site and to drive the positively charged ammonium ions to the exterior of the enzyme.

The Dimer Interface—The total contact area at the dimer interface is 1530 Å^2, being in the range of the contact extents in the other NrfA structures. The main interaction occurs at helix h23 that packs against h23 and h21 from the other monomer. The N terminus region of helix h21 establishes also an interaction with the short α-helix h18 (residues 307 to 314) at the opposite side of the dimer interface. Another interaction occurs between the additional helices h24 (residues 465 to 470) from both monomers, at the top of the dimer interaction region. The overall interaction is mainly hydrophobic but there is also an electrostatic contribution. The main hydrophobic interactions occur at the contact region of helices h23 and h24 with their ncs symmetry-related mates. However, there is an important electrostatic contribution in the interaction at helix h21 that involves a set of basic residues in this region interacting with negatively charged groups from the other monomer. This interaction involves Lys-356 from the loop at the N terminus of h21, and Arg-364, Lys-371, Lys-378, and Lys-385 from h21 that interact, respectively, with the propionate D from heme 5*, Asp-307* at h18*, and Asp-441*, Glu-448*, and Asp-455* at h23* at the other side of the dimer interface. This contact region is located near the product outlet and, in this way these charged residues make an important contribution to the electrostatic potential in that region. In the monomer alone the electrostatic potential will have only the contribution from the positively charged residues at h21, suggesting that dimer formation is important for creating the negative electrostatic potential around the product outlet.

The Active Site—The active site environment of *D. desulfuricans* NrfA is conserved, with Lys-150 as the proximal axial ligand of the iron in the penta-coordinated heme 1 (Fig. 4*A*). At the distal side of the active site, a blob of electron density in the electron density map could be interpreted as a water molecule bound to the heme iron at a distance of 2.1 Å and H-bonded to the Nϵ-2 of His-299 with a bond distance of 2.7 Å. His-299 at the distal side of the active site is conserved and its conformation corresponds to a generously allowed region of the Ramachandran plot as it happens in the other NrfA structures.

of the monomers of NrfA from *S. deleyianum*, *W. succinogenes*, and *E. coli* represented in *gray*, *blue*, and *green*, respectively, in the same orientation as in *C*. *E*, close up view of the putative product outlet. The narrowing of the product outlet channel is caused by the hydrophobic interaction between Leu-377 and Pro-97 and between Phe-373 and the main chain at His-94. The putative exit pathway for the ammonium ions is lined by the side chains of Tyr-73, Phe-92, and Phe-373 and is hindered by the side chains of Lys-93 and His-94. Figures were produced with programs Molscript and Raster3D (52, 53).

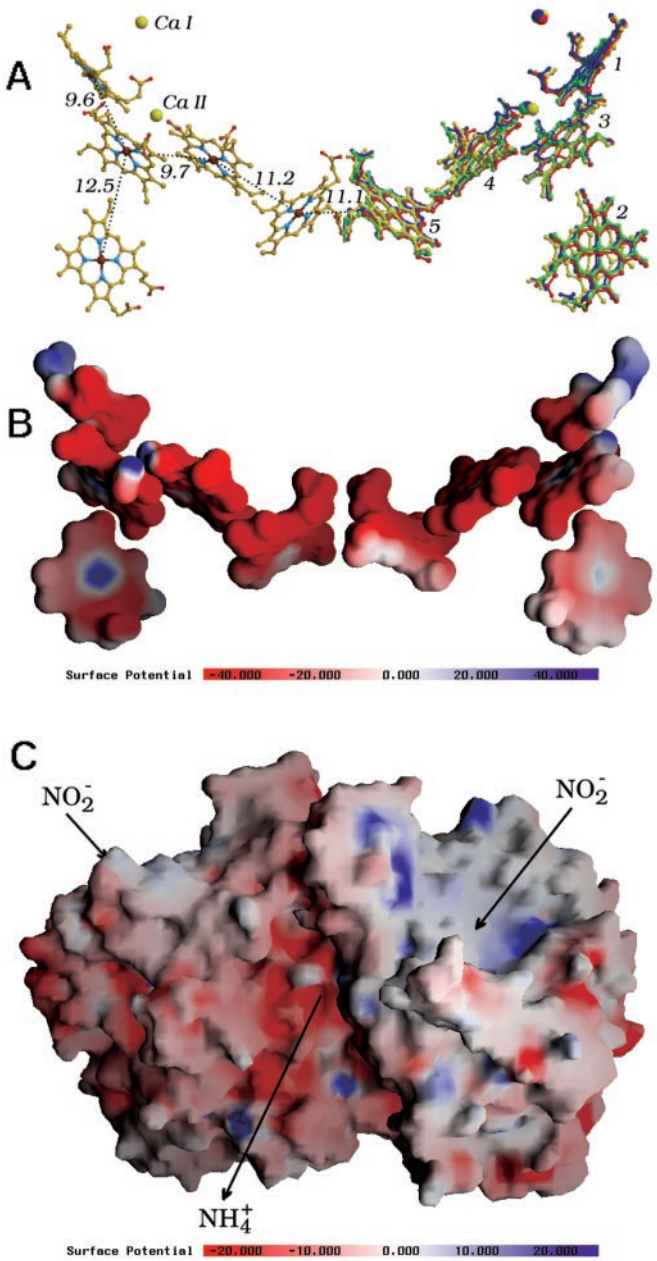

FIG. 3. *A*, the arrangement of the hemes and calcium sites in the dimer of *D. desulfuricans* NrfA is shown in the same orientation as in Fig. 2*A*, colored by atom type and as *yellow* on the *left-* and the *right-hand sides*, respectively. On the *right-hand side*, the superposition of the arrangements of the hemes and the calcium sites in the monomers of the NrfA structures from *S. deleyianum*, *W. succinogenes*, and *E. coli* is shown. The coloring scheme is according to the one used in Fig. 2*D* with the exception of *S. deleyianum* NrfA, which is colored *red*. The hemes are numbered according to the order of their binding motifs in the protein chain. The distances between the iron atoms are given in Å. In *D. desulfuricans* NrfA, the distance of calcium I to the iron atom of the active site (heme 1) is 10.7 Å and the calcium II ion is located at distances of 9.2, 10.6, and 12.6 Å from the iron atoms of hemes 3, 4, and 1, respectively. *B*, electrostatic potential mapped at the heme surfaces. The calculations were done on the dimer structure, considering the relative dielectric constant as 4.0 and 80.0 for the inner and outer regions of the protein, respectively. The electrostatic potential scale is given in millivolt units. The view is from opposite sides of the monomer not lacking the loop formed by residues 325 to 331 that is located in the vicinity of heme 2. The solvent accessibilities of the hemes determined from the structure are 34.0, 96.0, 2.5, 3.0, and 70.0 $Å^2$ for hemes 1, 2, 3, 4, and 5, respectively, and their experimentally determined redox potentials are −80, −50, −480, −400, and +150 mV, respectively.[1] *C*, electrostatic potential mapped at the dimer surface in an orientation slightly rotated clockwise around the non-crystallographic dyad and rotated to the front relatively to the view in Fig. 2*A*. The electrostatic potential scale is given in millivolt units. *Arrows* indicate the substrate inlet in both monomers and the product outlet in the monomer in the *left-hand side*. *A* was produced with programs Molscript and Raster3D (52, 53). *B* and *C* were done with GRASP (17).

The other residues present at the distal side of the active site, Arg-130 and Tyr-237, are also conserved. In addition to Tyr-237, the cavity of the active site is lined by a set of aromatic side chains that are also conserved within the NrfA structures: these include Tyr-106, Phe-108, Tyr-112, and Phe-239. Among these residues, Tyr-237 and Phe-239 in close proximity to the heme may have an important influence in its redox potential, because this is largely affected by the dielectric constant of the heme crevice (34). This in turn is affected by the solvent accessibility of the heme and the polarity of the surrounding environment. Aromatic amino acids in the immediate surroundings of hemes were shown to be important in the modulation of the redox potential in cases such as in the yeast iso-1-cytochrome *c* and the heme 4 of cytochrome c_3 (M_r 26,000) (35, 36). Near Tyr-237, a set of conserved tyrosine residues, Tyr-238, Tyr-266, and Tyr-267, have been suggested to play a role in dealing with possible radical intermediates during the reduction of nitrite to ammonia, a hypothesis supported by the observation of partial *ortho*-hydroxylation of Tyr-219 (corresponding to Tyr-238 in *D. desulfuricans* NrfA) in the structure of *W. succinogenes* NrfA (11).

Based in the B-factors and in the difference electron density maps, a spherical blob of electron density near the side chain of Arg-130 was assigned to a chloride ion, acting as a counterion at 3.6 Å from the Nϵ atom of the arginine. The presence of this ion probably arises from the use of $CaCl_2$ in the crystallization conditions. The side chain of Arg-130 is H-bonded to the propionate A of the active site heme at its distal side. The presence of the chloride ion near Arg-130 suggests that the shared proton in the H-bond between the side chain of the arginine and the propionate A of the active site heme is mainly kept at the arginine maintaining its positive charge. The crystal structure of *W. succinogenes* NrfA complexed with the substrate shows that nitrite bound at the active site is stabilized by H-bonds with the distal arginine and histidine (37), which suggests that the positive charge of the arginine may play an important role in the binding of nitrite to the active site.

Calcium Site Calcium I—The characteristic calcium ion near the active site (calcium I) is also conserved in *D. desulfuricans* NrfA (Fig. 4*A*), being located at a distance of 10.7 Å from the iron atom of heme 1 of the active site. The calcium ion is coordinated by Oϵ-1 and Oϵ-2 from Glu-236, the Oϵ-1 of Gln-298, and by the main chain carbonyls of Tyr-237 and Lys-296 at distances of 2.4 Å. Two waters H-bonded to the Oδ-1 and Oδ-2 of Asp-284 complete the coordination sphere of the calcium ion with bond distances of 2.5 and 2.4 Å, respectively. His-299 at the distal side of the active site heme is structurally coupled to this calcium ion by means of its coordination to the main chain carbonyl of Lys-296 and to the side chain of Gln-298 (Fig. 4*A*), residues contiguous to His-299 in the polypeptide chain. The calcium I calcium ion is also structurally coupled to His-234, the proximal axial histidine of heme 3, by means of its coordination by the side chain of Glu-236 and the main chain carbonyl of Tyr-237, residues contiguous to His-234 in the polypeptide chain (Fig. 4*A*). Furthermore, the Nδ-1 atom of this histidine is H-bonded to Glu-301, which is contiguous to His-299 in the polypeptide chain and so is also structurally coupled to this calcium ion.

Calcium Site Calcium II—In the N-terminal region of *D. desulfuricans* NrfA, residues from 68 to 76 constitute an additional loop (loop L1 in Fig. 2, *C* and *E*) that cages a clearly

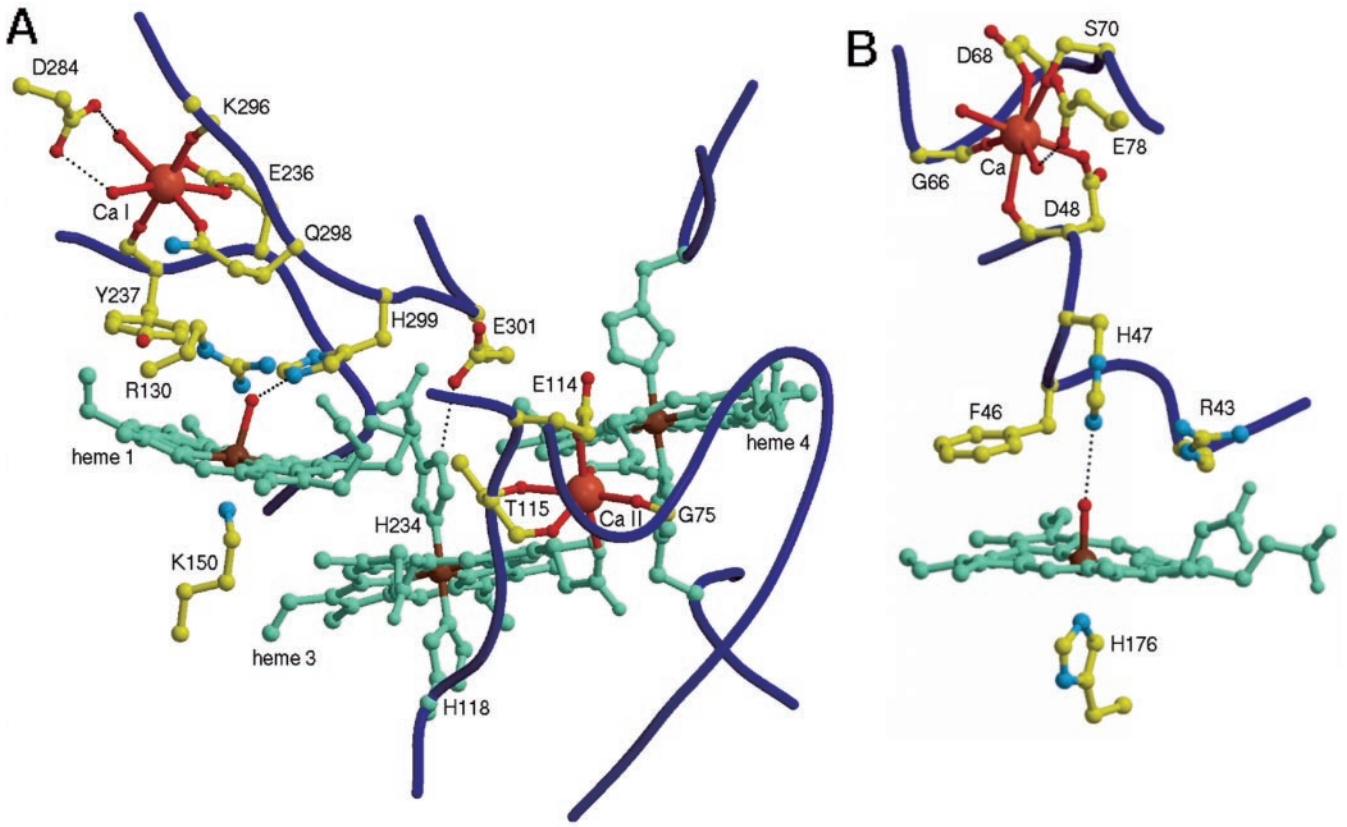

FIG. 4. *A*, the active site environment and the two calcium ions. At the active site, the electron density at the distal side of heme 1 could be interpreted as a water molecule coordinated to the iron atom. The structural coupling of the calcium sites to both axial histidines of heme 3 is shown. *B*, the active site of *P. chrysosporium* lignin peroxidase isoenzyme H2 and the distal calcium site characteristic of the class II and class III mono-heme peroxidases. The calcium ion is structurally coupled to the distal histidine at the active site in a similar manner as happens in the NrfA enzymes: it is coordinated by a main chain carbonyl group and a side chain belonging to residues in the polypeptide chain that are contiguous to the histidine at the distal side of the heme. Surprisingly, the deviation between the locations of the calcium sites in the superposition of the active sites (by superposing the hemes) of *P. chrysosporium* lignin peroxidase isoenzyme H2 and *D. desulfuricans* NrfA is only 5.5 Å (picture not shown). Also, the environment at the distal side of the active site heme is similar in these types of enzymes: a histidine, an arginine, and an aromatic residue are present in both cases. Figures were produced with programs Molscript and Raster3D (52, 53).

defined calcium ion (calcium II) with octahedral coordination. The presence of this loop constitutes a remarkable structural difference relative to the previous NrfA structures, whereas the presence of this calcium site was detected only in the case of the *E. coli* enzyme but without attributing any role to it. Two of the calcium ligands are the propionates A of both hemes 3 and 4 (Figs. 4*A* and 5*A*). The coordination sphere is completed by the main chain carbonyls of Gly-75, from the caging loop L1, and of Thr-115 as well as the side chains of Glu-114 and Thr-115. All the ligands are at distances of 2.4 Å from the calcium ion and this site is located at distances of 9.2, 10.6, and 12.6 Å from the iron atoms of hemes 3, 4, and 1, respectively. Whereas the proximal histidine of heme 3 is structurally coupled to the calcium I ion (as described above), the distal histidine of that heme (His-118) is structurally coupled to the calcium II ion by means of its coordination to the side chains of Glu-114 and Thr-115 as well as to the main chain carbonyl group of Thr-115.

In *E. coli* NrfA this calcium site is exposed because of the absence of the loop L1 that is absent in all the previous NrfA structures, and was reported to be coordinated to the propionates of hemes 3 and 4 as well as to the carbonyl group of Pro-91. It presented an incomplete coordination sphere with a water molecule as a fourth ligand (Fig. 5*C*) and no biological relevance was assigned to it at that time. There is some evidence for the existence of this calcium site also in the structure of *W. succinogenes* NrfA, but present as a Y^{3+} ion arising from the use of YCl_3 as an additive in the crystallization conditions. The Y^{3+} was also coordinated to the A propionates of hemes 3 and 4 and to the main chain carbonyl group of Pro-99. The other coordinating positions are occupied by three water molecules and by an acetate molecule (Fig. 5*B*). The only structure where this site was not observed was the one from *S. deleyianum* where the propionate A of heme 3 is in a different conformation making a H-bond with the main chain carbonyl group of Val-320 (Fig. 5*D*), but that may be because of the fact that calcium was not present in the crystallization conditions in this case.

Putative Substrate Inlet—The substrate inlet is surrounded on one side by the non-conserved C-terminal region composed of the short helices h26, h27, and h28 and the loop leading to the short β-sheet at the C terminus (Fig. 2*C*). On the opposite side, the substrate inlet is surrounded by three anti-parallel β-sheets: β1,2, β3,4, and β5,6. The polypeptide segment that forms β3,4 is non-existent in the previous NrfA structures (Fig. 2, *C* and *D*). Additionally, in NrfA from *S. deleyianum* and *W. succinogenes*, β1,2 is longer extending to the exterior of the enzyme. These structural differences in the β-sheet structure as well as in the non-conserved C-terminal region make the protein surface around the substrate inlet steeper in the case of *D. desulfuricans* NrfA. However, the electrostatic characteristics of the protein surface in this region are very similar to those of the other NrfA structures, namely the positively charged patch around the substrate channel (Fig. 3*C*).

Putative Product Outlet—The exit of the channel for the release of the product identified in the previous structures is partially blocked in *D. desulfuricans* NrfA. In this case, on one

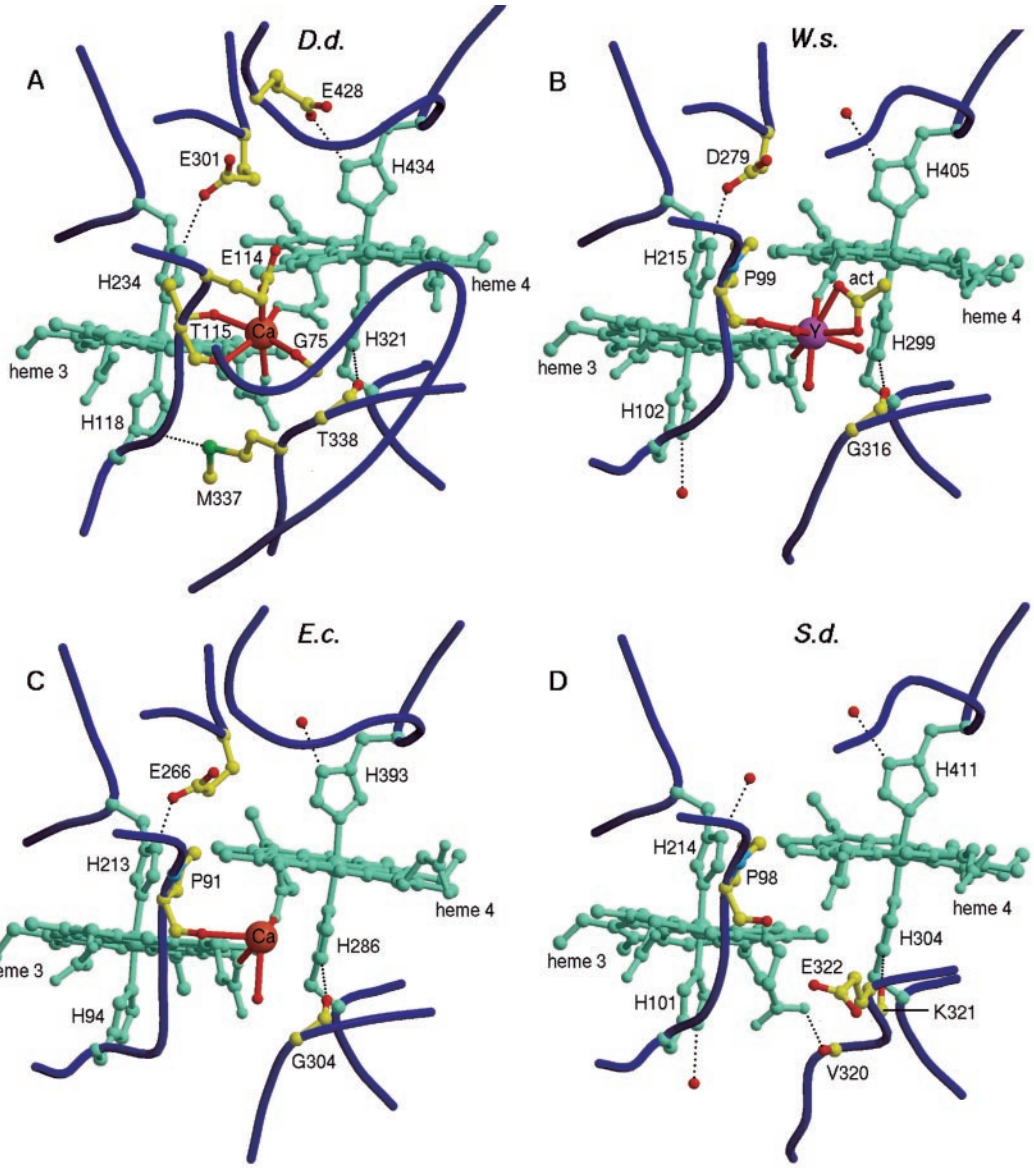

FIG. 5. **The calcium II site and the environments of hemes 3 and 4 in the NrfA structures of *D. desulfuricans* (*A*), *W. succinogenes* (*B*), *E. coli* (*C*), and *S. deleyianum* (*D*).** The calcium ion is present in the structures from *D. desulfuricans* and *E. coli* but poorly defined in the latter. In *W. succinogenes* NrfA a yttrium ion is present at this site with an acetate (*act*) ligand in its octahedral coordination sphere. The proximal histidine of heme 3 is H-bonded to a carboxylic side chain in NrfA from *D. desulfuricans, E. coli*, and *W. succinogenes* but not in *S. deleyianum* NrfA. The distal histidines of hemes 3 and 4 are H-bonded to a methionine and a carboxylic side chain, respectively, only in *D. desulfuricans* NrfA. Figures were produced with programs Molscript and Raster3D (52, 53).

side of the product outlet, there is a loop constituted by residues 84 to 94 that corresponds to an insertion in the protein sequence relative to the previous NrfA structures (loop L2 in Fig. 2*C*). This polypeptide segment has hydrophobic character and forms a one turn 3_{10} helix that interacts with Phe-373 from helix h21 at the opposite side of the product outlet. This interaction is hydrophobic involving the side chain of Phe-373 that interacts with both the Cα atom and the main chain carbonyl group of His-94, and the main chain carbonyl group of Ala-95, blocking this region of the channel (Fig. 2*E*). Phe-373 as well as the nearby Leu-376 are substituted by hydrophilic residues in the other NrfA structures. In one of the monomers, His-94 at loop L2 is coordinating a tetrahedral metal center by its Nϵ-2 atom at a distance of 2.1 Å. This metal center is located at an intermolecular contact with another copy of the same monomer related by crystallographic symmetry. The symmetry mate provides as additional ligands the Nδ-1 atom of His-399* and the Oδ-2 atom of Asp-462* at 2.1 and 2.0 Å, respectively. A fourth ligand was assigned to a chloride ion at a distance of 2.3 Å from the metal center and in contact with the Nζ atom of Lys-93 at a distance of 3.4 Å. Electron density maps calculated using the anomalous signal at the iron absorption edge (λ = 1.7390 Å) indicate that the metal cannot be iron. Considering the type of ligands coordinating it, one possibility is a zinc ion probably present as a residual contaminant of the reagents used for crystallization. The intermolecular contact originating this metal center does not exist in the crystal packing of the other monomer that, however, shows the same conformation for loop L2 that blocks the product channel. This fact suggests that this crystal contact most probably is a crystallization artifact and it is not responsible for the conformation of loop L2. Therefore this conformation will probably correspond to the one in solution. This is also supported by the fact that the interaction between this loop and Phe-373 from helix h21, responsible for hindering the putative product channel, is a hydrophobic interaction that will be favored in aqueous solution. However, the

absence of an obvious alternative channel for the release of the product as well as the conserved negative electrostatic potential in this region suggests that it functions as the outlet for the release of the ammonium ions also in *D. desulfuricans* NrfA. The loop partially blocking the product outlet in *D. desulfuricans* NrfA suggests that some dynamic behavior of the structure in this region is necessary for the release of the product. One feasible path for this is through the narrow channel lined by the aromatic side chains of Tyr-73, Phe-92, and Phe-373 (Fig. 2*E*), hindered by the side chain of His-94 that must move away to allow the release of the ammonium ions. Some dynamic behavior of the side chain of the nearby Lys-93 as well as of the main chain of loop L2 at residues Lys-93 and His-94 and of loop L1 at residue Tyr-73 may also be necessary. The interaction between the π-orbitals of the aromatic side chains surrounding this channel and the ammonium protons may play a role in driving the ammonium ions to travel through the channel. H-bond formation between the ammonium ions and the side chain of His-94 may also occur as a last step to assist the release of the product.

DISCUSSION

The Calcium I Site and Comparison to Mono-Heme Peroxidases—Despite the lack of sequence and structural homology, the environment of the vacant distal side of the active site heme of cytochrome *c* nitrite reductases is very similar to the environment of the distal side of the active site in the monoheme peroxidases such as cytochrome *c* peroxidase and fungal, plant, and horseradish peroxidases (38–43). In both types of enzymes, a histidine and an arginine are conserved near the free axial coordinating position at the distal side of the active site heme. In both cases, a reduction reaction of an oxygen-containing substrate occurs at the heme: nitrite is reduced to ammonia in cytochrome *c* nitrite reductase while hydrogen peroxide is reduced to water in the peroxidases. The active site has evolved independently in these two families of enzymes to a similar solution for similar biological processes.

Mutational and kinetic studies established a key role for the distal arginine in the active site of peroxidases in the rapid binding of the substrate to the active site and in the cleavage of the O–O bond (44, 45). In the structure of the horseradish peroxidase-cyanide complex the distal arginine H-bonds the bound cyanide, thereby contributing to the stabilization of the complex (46). A similar interaction was proposed to be involved in the stabilization of the bound peroxy transition state during O–O bond cleavage. Recently, in the structures of the complexes of cytochrome *c* nitrite reductase with nitrite and hydroxylamine, it was observed that the distal arginine also establishes H-bonds with the nitrite and hydroxylamine bound in the active site (37). This fact suggests a similar role of the distal arginine in the NrfA enzymes in the binding of the substrate and in the stabilization of the transition states of the various intermediate products in the reduction of nitrite to ammonium.

Class II peroxidases such as the fungal peroxidases as well as class III peroxidases such as the peanut and horseradish peroxidases contain two structural calcium ions. One of these calcium ions is located near the active site at its distal side and is surprisingly similar to the calcium I site in the NrfA enzymes (Fig. 4, *A* and *B*). This calcium ion in the peroxidases is structurally coupled to the distal histidine at the active site in a similar manner as happens in the NrfA enzymes as described above. In both cases, the calcium ion is coordinated by a main chain carbonyl group and a side chain belonging to residues in the polypeptide chain that are contiguous to the histidine at the distal side of the heme (Fig. 4, *A* and *B*). Despite the fact that the structure is not conserved, the location of these calcium sites relatively to the active site heme is similar in both types of enzymes as is illustrated by the deviation of only 5.5 Å between the locations of these calcium sites in the superposition of the active sites of *Phanerochaete chrysosporium* lignin peroxidase isoenzyme H2 and *D. desulfuricans* NrfA by superposing the hemes (picture not shown). For the lignin peroxidase as well as for the manganese peroxidase from *P. chrysosporium* (47, 48) it was shown that the release of this calcium ion from the structure resulted in the inactivation of the enzyme and this was related with the fact that upon release of the calcium ion the heme becomes coordinated by the histidine at the distal side. The coordination spheres of the calcium sites in these peroxidases are similar to the ones of the calcium I site in the NrfA enzymes. In both cases, the calcium sites are partially exposed to the solvent, and are coordinated by two water molecules and two main chain carbonyl groups. The coordination sphere is completed by the side chains of two aspartates and one serine in the case of the peroxidases, while in the NrfA enzymes the side chains of one glutamate and one glutamine are the additional ligands. These facts suggest that the binding constants for these calcium sites may be of similar magnitudes, and therefore that the calcium ion at the calcium I site in the NrfA will be strongly bound to the protein as happens in the case of the peroxidases.

The high similarity between the distal calcium ion near the active site in the peroxidases and the calcium I site in the NrfA enzymes suggests that the release of this ion in the NrfA enzymes will have the same structural consequences that are observed for the peroxidases. Apart from the contribution to the positive electrostatic potential at the active site cavity, the calcium I ion in the NrfA enzymes may play an important role in keeping the distal histidine away from the iron atom at the active site heme for the enzyme to be active. Previously reported studies regarding the influence of calcium in the activity of the NrfA enzymes from *S. deleyianum* and *E. coli* do not refer to the complete loss of activity of the enzyme in the absence of calcium ions in solution (13, 49) contradicting the above hypothesis. However, the way these studies were carried out suggests a labile character of the putative calcium site involved. For this reason, the calcium II site may be the one involved in the effects observed in the NrfA activity in these studies. Because of its incomplete coordination sphere in the case of NrfA from *S. deleyianum* and *E. coli* as well as in *W. succinogenes* (Fig. 5, *B–D*), the calcium II calcium site may be expected to be labile in these cases. On the other hand, the coordination sphere of the calcium I site (Fig. 4*A*) suggests that it will be strongly bound to the protein and very difficult to be released as happens in the case of the peroxidases. The effects reported in the above studies were not interpreted according to the existence of the calcium II site maybe because this site was not clearly revealed at that time. A calcium ion was not present at this site in the *S. deleyianum* NrfA structure, the first NrfA structure reported. However, as already mentioned above, the crystallization conditions in this case did not contain calcium ions and, for this reason, the existence of this calcium site also in *S. deleyianum* NrfA cannot be excluded.

The Calcium II Site—There is some evidence for the existence of the calcium II site also in the crystal structures of NrfA from *E. coli* and *W. succinogenes.* However, in these cases the ions are located at the protein surface and only three protein ligands are present in their coordination spheres: both the propionates A of hemes 3 and 4 and a main chain carbonyl group, being the other coordination positions exposed to the solvent. In *D. desulfuricans* NrfA this calcium site is identified for the first time with complete octahedral coordination by protein ligands (Fig. 5*A*). In this case, the additional ligands are the main chain carbonyl group of Gly-75 and both side

chains of Glu-114 and Thr-115. In NrfA from *E. coli* and *W. succinogenes*, Glu-114 and Thr-115 are mutated to residues whose side chains are unable to coordinate the calcium. Additionally Gly-75 in *D. desulfuricans* NrfA belongs to a loop that is non-existent in the other NrfA structures (Fig. 5, *B–D*). The fact that the calcium II ion is firmly bound by protein ligands in nearly perfect octahedral coordination in *D. desulfuricans* NrfA suggests that it may play an important physiological role arising either from an electrostatic effect, because of its positive charge, or simply from structural effects. From these, perhaps the most obvious effect will be the conformation of the additional loop that coordinates the calcium ion and that exerts influence in the solvent accessibility to the interior of the protein, namely to the cavity of heme 4. Both effects can influence the redox potential of the hemes involved.

To evaluate the electrostatic effect of the charge of the calcium ion at the calcium II site in the nearby hemes, the electrostatic potential arising from the charged groups in the protein structure was mapped at the surface of the hemes (Fig. 3*B*). The electrostatic potential was calculated without considering the presence of the membrane anchoring subunit (NrfH) whose structure is not known. The presence of this subunit will influence the electrostatic potential in the vicinity of hemes 2 and 5, which are located near the putative binding region of that subunit. For this reason, the electrostatic potentials mapped at the surface of these hemes may be different from the ones at the physiological conditions, in the NrfHA complex. However, despite the absence of the NrfH subunit, the electrostatic potentials mapped at the surface of hemes 1, 3, and 4 are expected to be a good approximation of the electrostatic potential in the physiological conditions, because these hemes are more distantly located from the binding region of the NrfH subunit. The results show that the active site heme 1 is partially subjected to positive electrostatic potential that arises from the positively charged residues that line the substrate channel. On the contrary, hemes 3 and 4 near the product outlet are subjected to strongly negative electrostatic potential. This is in accordance with the change from positive to negative electrostatic potential along the channel that traverses the monomer from the substrate inlet to the product outlet as has been reported in previous structures (11). In the left-hand side of Fig. 3*B*, it can be observed that the positive electrostatic potential arising from the calcium ion at the calcium II site is restricted to the regions of the propionates involved in its coordination, whereas the porphirin rings of hemes 3 and 4 are subjected to strong negative electrostatic potential. This fact suggests that the negative electrostatic potential in the heme cavities overwhelms the positive electrostatic contribution of the calcium ion being in accordance with the highly negative oxidation-reduction potentials assigned to these hemes. Combining information from potentiometric titrations and EPR and Mössbauer spectroscopic studies, the oxidation-reduction potentials of hemes 3 and 4 were assigned the redox potentials of −480 and −400 mV,[1] respectively. These redox potentials reflect the destabilization of the reduced state of the heme because of the influence of the strong negative electrostatic potentials at the heme cavities, despite the presence of the calcium ion near the propionates of the hemes. These facts suggest that the main influence of this calcium site in the redox potential of the nearby hemes will not be the electrostatic effect.

The calcium ion at the calcium II site may also have an important structural role, namely in stabilizing the conformation of the loop formed by residues 68 to 76 (loop L1 in Fig. 2*C*) by means of its coordination to the calcium ion by the main chain carbonyl group of Gly-75. The very low solvent accessibility of heme 4 in *D. desulfuricans* NrfA (3.0 $Å^2$) compared with the high solvent accessibilities reported for this heme in the previous NrfA structures lacking the loop L1 (61.7 to 83.6 $Å^2$) (12), suggests that the presence of this loop in *D. desulfuricans* NrfA exerts a strong influence in the solvent accessibility of this heme. Heme 3 also presents a very low solvent accessibility (2.5 $Å^2$) but this also happens in the previous structures (2.5 to 17.5 $Å^2$). The low solvent accessibility of the cavities of hemes 3 and 4 suggests that the dielectric constant of the environment around these hemes will be low. This fact will tend to increase the effect of the negative electrostatic influence in the hemes increasing the destabilization of the reduced state and this may explain the highly negative redox potentials determined for these hemes. In this way, the low solvent accessibility of heme 4, caused by the loop L1, and the consequent low dielectric constant of the environment around that heme may exert a more effective influence in the redox potential of the heme than the electrostatic charge of the calcium ion caged by the loop. Furthermore, the heme propionates that coordinate the calcium ion may become protonated in its absence reducing the electrostatic effect caused by the absence of the positive charge of the calcium ion. These facts suggest that the role of the calcium II ion may be of structural nature, by stabilizing the conformation of the loop L1, rather than an electrostatic effect caused by its positive charge.

Another factor that may influence the redox potential of hemes 3 and 4 is the type of the acceptor group of the H-bonds formed by the axial histidines of those hemes. In *D. desulfuricans* NrfA, the Nδ-1 atoms of the proximal histidine of heme 3 (His-234) and the distal histidine of heme 4 (His-434) are H-bonded by the carboxylic side chains of Glu-301 and Glu-428, respectively (Fig. 5*A*). The H-bond interaction between axial heme histidines and carboxylic side chains has been shown to influence the redox potential of hemes (50). The carboxylate is supposed to deprotonate partially or completely the histidine to form the imidazolate thus increasing the strength of the histidine-iron bond and shifting downwards the redox potential of the heme. The negative shift of the redox potential of the heme was shown to depend on the geometry of the H-bond interaction, namely the C = O–H angle defined by the hydrogen riding the Nδ-1 atom of the histidine and the carbonyl group of the H-bonded carboxylic function. The maximum effect reported was achieved for an ideal geometry corresponding to a C = O–H angle of 120° causing a shift of about −100 mV in the redox potential of the heme. This effect contributes also for the highly negative redox potentials assigned to hemes 3 and 4, being another factor counteracting the influence of the positive charge of the calcium ion at the calcium II site on those redox centers. Additionally, changes in the geometry of the H-bonds between the Nδ-1 atoms of the histidines and the carboxylic groups, because of dynamical behavior of the protein structure, may provide a means for a dynamic modulation of the potential of the hemes involved.

On the contrary to what happens with the other heme axial histidines, the acceptor group for the H-bonds formed by the Nδ-1 atom of both axial histidines of heme 3 and the distal histidine of heme 4 are not conserved in the NrfA enzymes. The proximal histidine of heme 3 is H-bonded to a carboxylic side chain in the NrfA structures from *D. desulfuricans*, *W. succinogenes*, and *E. coli* but not in the one from *S. deleyianum* (Fig. 5, *A–D*). On the other hand, the distal histidine of heme 3 is H-bonded to water molecules in all the currently known structures with the exception of the one from *D. desulfuricans* where it is unusually H-bonded to the sulfur atom of a methionine side chain (Met-337). The distal histidine of heme 4 is also H-bonded to water molecules in all the previous structures but

it is observed to make a H-bond to a carboxylic side chain (Glu-428) in the case of *D. desulfuricans* NrfA. In contrast to this, the H-bonding to the Nδ-1 atom of the axial histidines of hemes 2 and 5 has been conserved in the NrfA structures. With the exception of the proximal histidine of heme 5, at the dimer interface, which is H-bonded to the propionate D of the ncs-related heme 5* at the opposite side of the dimer interface, the other heme axial histidines are H-bonded to main chain carbonyls or water molecules. The non-conserved H-bonds between the axial histidines of hemes 3 and 4 and carboxylic side chains that are observed in some of the NrfA structures may be a factor involved in the tuning of the redox potential of those hemes, as referred above. The variability of this structural motif within this family of enzymes reflects the variability of the environment around those hemes, mainly in the region closer to the putative product outlet, a region with a low degree of conserved residues, in contrast with the highly conserved region of the active site cavity. To test these hypotheses additional theoretical and experimental work must be done and is planned in the near future.

Acknowledgments—We thank Cláudio Soares (Instituto de Tecnologia Química e Biológica, Oeiras, Portugal) for fruitful discussions and Oliver Einsle (MPI Biochemie, Martinsried, Germany) for providing the coordinates of NrfA from *S. deleyianum* when they were not available at the Protein Data Bank and the supporting staff at beamlines BM-14 and ID14-EH4 are also acknowledged.

REFERENCES

1. Liu, M. C., and Peck, H. D., Jr. (1981) *J. Biol. Chem.* **256,** 13159–13164
2. Steenkamp, D. J., and Peck, H. D., Jr. (1981) *J. Biol. Chem.* **256,** 5450–5458
3. Schröder, I., Roberton, A. M., Bokranz, M., Unden, G., Böcher, R., and Kröger, K. (1985) *Arch. Microbiol.* **140,** 380–386
4. Moura, I., Bursakov, S., Costa, C., and Moura, J. J. G. (1997) *Anaerobe* **3,** 279–290
5. Ferguson, S. J. (1998) *Curr. Opin. Chem. Biol.* **2,** 182–193
6. Simon, J. (2002) *FEMS Microbiol. Rev.* **26,** 285
7. Dias, J. M., Than, M. E., Humm, A., Huber, R., Bourenkov, G. P., Bartunik, H. D., Bursakov, S., Calvete, J., Caldeira, J., Carneiro, C., Moura, J. J., Moura, I., and Romao, M. J. (1999) *Struct. Fold. Des.* **7,** 65–79
8. Simon, J., Pisa, R., Stein, T., Eichler, R., Klimmek, O., and Gross, R. (2001) *Eur. J. Biochem.* **268,** 5776–5782
9. Simon, J., Gross, R., Einsle, O., Kroneck, P. M. H., Kröger, A., and Klimmek, O. (2000) *Mol. Microbiol.* **35,** 686–696
10. Einsle, O., Messerschmidt, A., Stach, P., Bourenkov, G. P., Bartunik, H. D., Huber, R., and Kroneck, P. M. H. (1999) *Nature* **400,** 476–480
11. Einsle, O., Stach, P., Messerschmidt, A., Simon, J., Kröger, A., Huber, R., and Kroneck, P. M. H. (2000) *J. Biol. Chem.* **275,** 39608–39616
12. Bamford, V. A., Angove, H. C., Seward, H. E., Thomson, A. J., Cole, J. A., Butt, J. N., Hemmings, A. M., and Richardson, D. J. (2002) *Biochemistry* **41,** 2921–2931
13. Stach, P., Einsle, O., Schumacher, W., Kurun, E., and Kroneck, P. M. H. (2000) *J. Inorg. Biochem.* **79,** 381–385
14. Costa, C., Macedo, A., Moura, I., Moura, J. J. G., LeGall, J., Berlier, Y., Liu, M. Y., and Payne, W. J. (1990) *FEBS Lett.* **276,** 67–70
15. Liu, M. C., Costa, C., and Moura, I. (1994) in *Inorganic Microbial Sulphur Metabolism* (Peck, H. D., Jr., and LeGall, J., eds) Vol. 243, pp. 303–319, Academic Press, Inc., London, UK
16. Costa, C., Moura, J. J. G., Moura, I., Wang, Y., and Huynh, B. H. (1996) *J. Biol. Chem.* **271,** 23191–23196
17. Nicholls, A., Sharp, K. A., and Honig, B. (1991) *Proteins* **11,** 281–296
18. Nielsen, H., Engelbrecht, J., Brunak, S., and von Heijne, G. (1997) *Protein Eng.* **10,** 1–6
19. Laemmli, U. K. (1970) *Nature* **227,** 680–685
20. Dias, J. M., Cunha, C. A., Teixeira, S., Almeida, G., Costa, C., Lampreia, J., Moura, J. J. G., Moura, I., and Romão, J. M. (2000) *Acta Crystallogr. Sect. D* **56,** 215–217
21. Otwinowski, Z., and Minor, W. (1997) in *Macromolecular Crystallography, Part A* (Carter, C. W., Jr., and Sweet, R. M., eds) Vol. 276, pp. 307–326, Academic Press, New York
22. Terwilliger, T. C., and Berendzen, J. (1999) *Acta Crystallogr. Sect. D* **55,** 849–861
23. La Fortelle, E. D., and Bricogne, G. (1997) in *Macromolecular Crystallography, Part A* (Carter, C. W., Jr., and Sweet, R. M., eds) Vol. 276, pp. 472–494, Academic Press, New York
24. Abrahams, J. P., and Leslie, A. G. W. (1996) *Acta Crystallogr. Sect. D* **52,** 30–42
25. Cowtan, K. (1994) *Joint CCP4 and ESF-EACBM Newsletter on Protein Crystallography* **31,** 34–38
26. Collaborative Computational Project, N. (1994) *Acta Crystallogr. Sect. D* **50,** 760–763
27. Navaza, J. (1994) *Acta Crystallogr. Sect. D* **50,** 157–163
28. Matthews, B. W. (1968) *J. Mol. Biol.* **33,** 491–497
29. Jones, T. A., Zou, J.-Y., Cowan, S. W., and Kjelgaard, M. (1991) *Acta Crystallogr. Sect. A* **47,** 110–119
30. Murshudov, G. N., Vagin, A. A., and Dodson, E. J. (1997) *Acta Crystallogr. Sect. D* **53,** 240–255
31. Perrakis, A., Morris, R. J., and Lamzin, V. S. (1999) *Nat. Struct. Biol.* **6,** 458–463
32. Hooft, R. W. W., Vriend, G., Sander, C., and Abola, E. E. (1996) *Nature* **381,** 272–272
33. Page, C. C., Moser, C. C., Chen, X., and Dutton, P. L. (1999) *Nature* **402,** 47–52
34. Kassner, R. J. (1973) *J. Am. Chem. Soc.* **95,** 2674–2677
35. Rafferty, S. P., Pearce, L. L., Barker, P. D., Guillemette, J. G., Kay, C. M., Smith, M., and Mauk, A. G. (1990) *Biochemistry* **29,** 9365–9369
36. Aubert, C., Leroy, G., Bruschi, M., Wall, J. D., and Dolla, A. (1997) *J. Biol. Chem.* **272,** 15128–15134
37. Einsle, O., Messerschmidt, A., Huber, R., Kroneck, P. M. H., and Neese, F. (2002) *J. Am. Chem. Soc.* **124,** 11737–11745
38. Poulos, T. L., Freer, S. T., Alden, R. A., Edwards, S. L., Skogland, U., Takio, K., Eriksson, B., Xuong, N., Yonetani, T., and Kraut, J. (1980) *J. Biol. Chem.* **255,** 575–580
39. Poulos, T. L., Edwards, S. L., Wariishi, H., and Gold, M. H. (1993) *J. Biol. Chem.* **268,** 4429–4440
40. Sundaramoorthy, M., Kishi, K., Gold, M. H., and Poulos, T. L. (1994) *J. Biol. Chem.* **269,** 32759–32767
41. Kunishima, N., Fukuyama, K., Matsubara, H., Hatanaka, H., Shibano, Y., and Amachi, T. (1994) *J. Mol. Biol.* **235,** 331–344
42. Schuller, D. J., Ban, N., Huystee, R. B., McPherson, A., and Poulos, T. L. (1996) *Structure* **4,** 311–321
43. Gajhede, M., Schuller, D. J., Henriksen, A., Smith, A. T., and Poulos, T. L. (1997) *Nat. Struct. Biol.* **4,** 1032–1038
44. Vitello, L. B., Erman, J. E., Miller, M. A., Wang, J., and Kraut, J. (1993) *Biochemistry* **32,** 9807–9818
45. Rodriguez-Lopez, J. N., Smith, A. T., and Thornley, R. N. (1996) *J. Biol. Chem.* **271,** 4023–4030
46. Henriksen, A., Smith, A. T., and Gajhede, M. (1999) *J. Biol. Chem.* **274,** 35005–35011
47. George, S. J., Kvaratskhelia, M., Dilworth, M. J., and Thorneley, R. N. F. (1999) *Biochem. J.* **344,** 237–244
48. Sutherland, G. R. J., Zapanta, L. S., Tien, M., and Aust, S. D. (1997) *Biochemistry* **36,** 3654–3662
49. Angove, H. C., Cole, J. A., Richardson, D. J., and Butt, J. N. (2002) *J. Biol. Chem.* **277,** 23374–23381
50. Goodin, D. B., and McRee, D. E. (1993) *Biochemistry* **32,** 3313–3324
51. Barton, G. J. (1993) *Protein Eng.* **6,** 37–40
52. Kraulis, P. J. (1991) *J. Appl. Crystallogr.* **24,** 946–950
53. Merritt, E. A., and Bacon, D. J. (1997) in *Macromolecular Crystallography, Part B* (Carter, C. W., Jr., and Sweet, R. M., eds) Vol. 277, pp. 505–524, Academic Press, New York